

Surface anisotropy and magnetic freezing of MnO nanoparticles

M. A. Morales,¹ R. Skomski,¹ S. Fritz,¹ G. Shelburne,¹ J. E. Shield,² Ming Yin,³ Stephen O'Brien,³ and D. L. Leslie-Pelecky¹

¹*Department of Physics and Astronomy and Nebraska Center for Materials and Nanoscience, University of Nebraska-Lincoln, Lincoln, Nebraska 68588-0111, USA*

²*Department of Mechanical Engineering and Nebraska Center for Materials and Nanoscience, University of Nebraska-Lincoln, Lincoln, Nebraska 68588-0656, USA*

³*Department of Applied Mathematics and Physics, Columbia University, New York City, New York 10027, USA*

(Received 5 February 2007; revised manuscript received 5 March 2007; published 26 April 2007)

Nanoparticles of bulk antiferromagnets often exhibit ferromagnetic behavior due to uncompensated surface spins. The peak temperature in the zero-field-cooled magnetization of MnO—in contrast to other antiferromagnetic nanoparticles—has anomalous behavior, shifting to *higher* temperatures with decreasing nanoparticle size. We attribute this behavior to surface anisotropy enhanced by the specific occupancy of $3d$ levels in Mn, which produces a high-spin–low-spin transition not present in NiO nanoparticles.

DOI: [10.1103/PhysRevB.75.134423](https://doi.org/10.1103/PhysRevB.75.134423)

PACS number(s): 75.50.Tt, 75.50.Ee, 75.70.Rf, 75.75.+a

I. INTRODUCTION

Antiferromagnetic nanoparticles often exhibit a net magnetic moment due to uncompensated surface spins, with the moment becoming larger as the surface-to-volume ratio increases. This surface magnetism affects other magnetic properties, such as the superparamagnetic blocking of the particles' spin magnetization directions. An unexplained phenomenon is that the temperature of the peak T_p in the zero-field-cooled (ZFC) magnetization $M_{ZFC}(T)$ of MnO nanoparticles shifts to *higher* temperatures with decreasing particle size.^{1–3} This temperature dependence is opposite that of most other antiferromagnetic nanoparticles, including the isostructural rocksalt oxide NiO.^{4–6} There is one report of anomalous T_p dependence in NiO; however, the samples were produced by a sol-gel technique and have a broad particle-size distribution that includes micron-sized agglomerates.^{7,8}

Superparamagnetic blocking, as measured by $M_{ZFC}(T)$, is commonly explained as an anisotropy effect. Large surface anisotropy can result from spin-orbit coupling in combination with the reduced symmetry of surface atoms, but Mn^{2+} has a half-filled $3d$ shell and ${}^6S_{5/2}$ ground state. This should not produce significant anisotropy, even in environments with reduced symmetry, such as strained crystals and at surfaces.^{9–12} Local disorder, however, permits occupancy of the $3d$ levels in Mn to produce a high-spin–low-spin transition that could be responsible for the anomalous shift of T_p with size.

II. EXPERIMENT

MnO nanoparticles were synthesized by thermal decomposition of manganese acetate in the presence of oleic acid at high temperature.¹³ The nanoparticles are suspended in hexane and stored under argon to prevent further oxidation. Samples were characterized by x-ray diffraction, transmission electron microscopy (TEM), and atomic absorption spectroscopy (AAS). The oleic acid coating and handling in a protected atmosphere prevents the formation of an oxide shell. The size dispersions for each sample are characterized

by a normal distribution, as shown in Fig. 1. The smallest nanoparticles (sample A) have a spherical to irregular shape with mean diameter 8.5 nm and $\sigma=2.4$ nm. Medium-sized particles (sample B) are cubic with mean cube-edge length 21.4 nm and $\sigma=2.2$ nm. Sample C contains square dipyramids or hexagonal prisms with a mean diameter of 42 nm and $\sigma=2.8$ nm. X-ray diffraction confirms the expected rocksalt structure with lattice constants 443.8 ± 0.1 pm (sample C), 443.4 ± 0.2 pm (sample B), and 443.4 ± 0.5 pm (sample

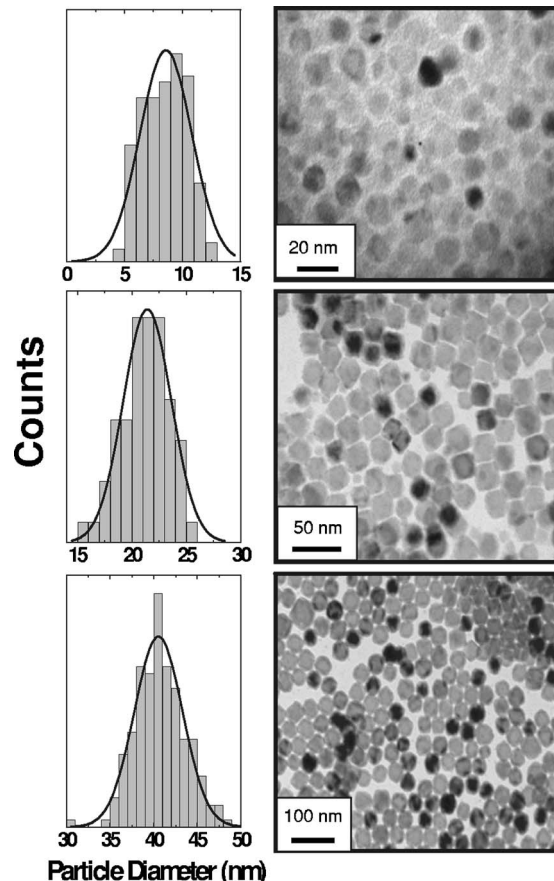


FIG. 1. Transmission electron micrographs and size distributions for (from top) samples A, B, and C.

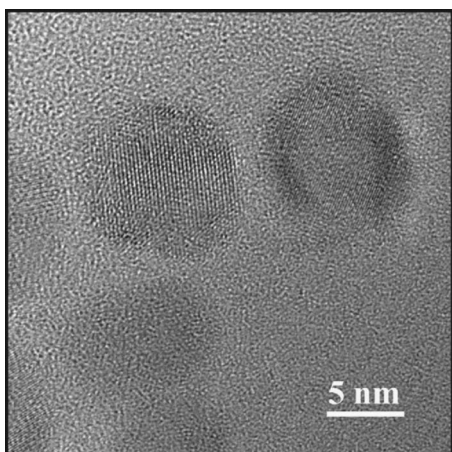


FIG. 2. A high-resolution transmission electron micrograph showing the single-crystal nature of the MnO nanoparticles.

A), each close to the MnO bulk value. The nanoparticles are single crystals, as shown by the high-resolution transmission electron micrograph in Fig. 2. No evidence of a Mn_3O_4 shell is observed by high-resolution TEM, electron diffraction, or in magnetic measurements. The lack of a shell is attributed to the oleic acid ligands at the nanoparticle surface and handling the samples only in inert atmospheres.

Nanoparticles for magnetic measurements were encapsulated in paraffin and sealed in polyethylene bags to prevent nanoparticle rotation during measurement and protect the samples from oxidation during transfer to the magnetometer. Nanoparticles frozen in hexane at varying dilutions also were measured to test for interparticle interactions; however, the results were similar to the paraffin-encapsulated samples. Magnetic data were normalized to the Mn mass obtained from AAS. Figure 3 shows the field-cooled (M_{FC} , open symbols) and zero-field cooled (M_{ZFC} , closed symbols) magnetizations measured at 100 Oe, yielding T_p 's of 27.4 ± 1.4 K (sample A), 21.7 ± 2.9 K (sample B), and 17.8 ± 3.5 K (sample C). The overall magnetization increases with decreasing size, consistent with the increasing number of uncompensated spins. A feature in the magnetization near

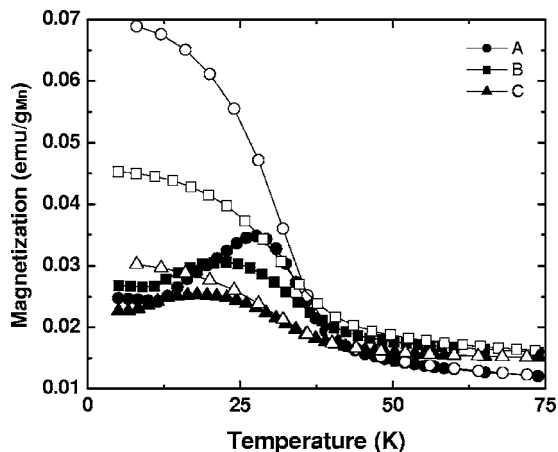


FIG. 3. The zero-field-cooled (closed symbols) and field-cooled (open symbols) magnetizations measured at 100 Oe.

118 K (the bulk Néel temperature of MnO) is observed only in the largest nanoparticles.

In the absence of magnetic fields, the net magnetization of an antiferromagnet is zero; however, an external field causes spin canting of order H/J , which adds to, and often overcompensates, the signal from uncompensated surface spins. The dependence of M on H generally is nonlinear due to the spin-flop transitions, so there is no simple way of subtracting this background from hysteresis loops.¹⁴ Hysteresis is observed at temperatures well above T_p , consistent with the onset of irreversibility between M_{FC} and M_{ZFC} . The coercivity increases significantly below the irreversibility temperature, reaching values of 0.7 T at 5 K for sample A. The ferromagnetic saturation magnetization is zero at temperatures above 50 K and increases below T_p . Despite the anomalous T_p behavior, MnO shows many similarities to NiO: For example, large shifts in the hysteresis loops are found after field cooling and the superparamagnetic contributions do not scale with H/T .⁶

III. MAGNETIC ANISOTROPY

As in other nanoparticle systems, T_p and the coercivity of our MnO nanoparticles are related directly to the magneto-crystalline anisotropy. Shape anisotropy is unimportant compared to magnetocrystalline anisotropy because the nanoparticles are roughly equiaxed and the net magnetization is very small. The magnetic anisotropy of low-indexed surfaces can be much higher than the cubic bulk anisotropy, as is known from ultrathin films.^{9–12} Surface anisotropy arises from reduced symmetry and spin-orbit coupling, which are present in other types of nanoparticles; however, surface anisotropy also requires suitable occupancy of the $3d$ levels.

Neither Mn^{2+} nor Ni^{2+} is expected to produce significant anisotropy. In lowest order, Mn^{2+} is an S -state ion with a half-filled shell and zero anisotropy. The t_{2g} and e_g levels of Ni^{2+} are fully occupied and half-occupied, respectively, with the anisotropy vanishing for each level. This is very different than the large anisotropy of other transition-metal ions, such as Co^{2+} in cobalt ferrites. The difference in the behavior of NiO and MnO nanoparticles originates in the different crystal-field splitting and level occupancy of these two ions.

A. Crystal-field splitting

Figure 4 compares the crystal-field levels of free $3d$ ions and $3d$ ions in an octahedral crystal environment (appropriate for bulk MnO and NiO) with the level splittings for $3d$ ions on ideal and imperfect (001) surfaces. For clarity, Fig. 4 shows the level splitting for *small* deviations from cubic symmetry; however, there are two additional effects. First, the $3d$ -band width of transition metal oxides often is comparable to or even somewhat larger than the crystal-field splitting.¹⁵ Second, the noncubic crystal-field distortion on moving the atoms to infinity is much larger than the cubic crystal field. In fact, creating an ideal surface, as indicated in Fig. 4, means that $|z^2\rangle$ becomes the lowest-lying level and that the splitting between the top $|x^2-y^2\rangle$ and bottom $|z^2\rangle$ levels is much larger than the e_g-t_{2g} splitting. Compared to

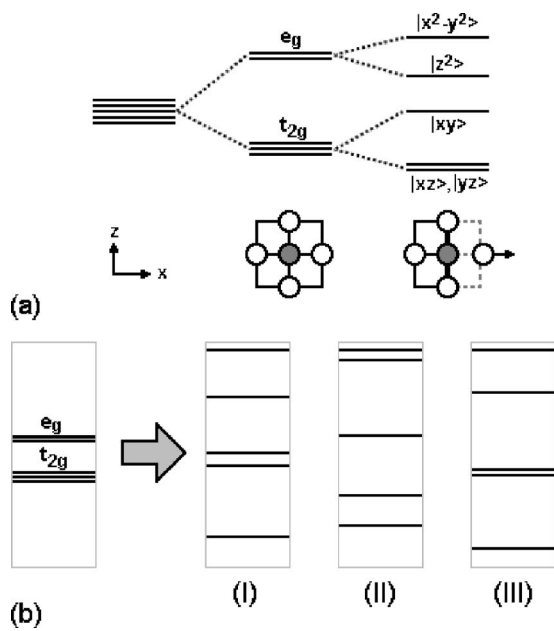


FIG. 4. Crystal-field splitting for $3d$ ions (dark) coordinated by oxygen atoms (white). Weak deviations from cubic symmetry (a) leave the levels reminiscent of the cubic e_g-t_{2g} splitting, whereas strong deviations (b) yield a complete remixture of the levels. The cases (I)–(III) are typical splittings at low-indexed surfaces, each corresponding to a different atomic environment.

fourth-order cubic terms, tetragonal and other second-order crystal-field contributions carry a factor of the order of $R_{T-O}^2/R_{3d}^2 \approx 6$, where $R_{T-O} \approx 2.1 \text{ \AA}$ and $R_{3d} \approx 0.85 \text{ \AA}$ are the interatomic distance and the $3d$ shell radius.¹⁶ This means that the behavior of surface atoms is determined largely by the crystal-field splitting.

The moment and (indirectly) the anisotropy of an ion in a crystalline environment reflect competition between exchange and crystal-field splitting. The crystal field favors low-spin configurations where $\uparrow\downarrow$ spin pairs occupy the low-lying crystal-field states. In most compounds, however, the intra-atomic exchange can create high-spin states having the largest spin compatible with the Pauli principle. In this regime, the filling of energy levels starts with \uparrow electrons at the expense of some crystal-field energy. The low-spin state in MnO no longer has a half-filled $3d\uparrow$ shell, which may produce magnetic anisotropy.

The commonly considered high-spin–low-spin transitions in octahedral crystalline environments are limited to configurations from $3d^4$ to $3d^7$. Three or fewer electrons are accommodated in the low-lying t_{2g} triplet, and there is no crystal-field gain on reducing the spin. For $3d^8$ to $3d^{10}$ configurations, the occupancy of low-lying crystal-field states is forbidden by the Pauli principle. For $4 \leq n \leq 7$ d electrons, the cubic crystal field usually is too weak to cause a high-spin–low-spin transition; however, Fig. 4 shows that this is no longer the case for crystal fields at surfaces, and special care is necessary to treat deviations from the e_g-t_{2g} splitting. Depending on the details of the level splitting, the Mn^{2+} may undergo two different types of high-spin–low-spin transitions, from a spin of $5\mu_B$ per atom to an intermediate state ($3\mu_B$) or to a proper low-spin state ($1\mu_B$). The large

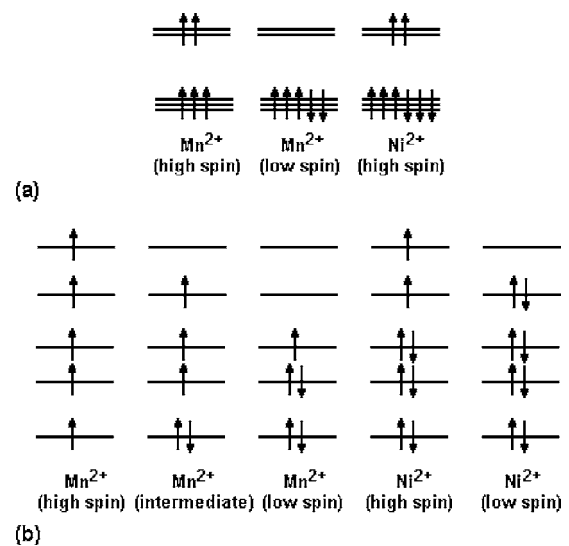


FIG. 5. Schematic level diagram of the high-spin and low-spin states of Mn^{2+} and Ni^{2+} : (a) octahedral symmetry and (b) most general case of low symmetry. In (b) the five singlets have random energies and cannot be labeled as in Fig. 4.

crystal-field splitting makes the second scenario more likely. As a consequence, the \uparrow shell is no longer filled, and the Mn may develop magnetic anisotropy. The Ni^{2+} ion may also exhibit a high-spin–low-spin transition; however, the resulting state has zero spin and zero anisotropy.

B. Magnetocrystalline anisotropy

Partially occupied levels coupled by spin-orbit coupling are required to create anisotropy.¹⁷ If two levels connected by spin-orbit coupling are occupied by two electrons, the net anisotropy is zero due to the cancellation of the orbital ($\uparrow\uparrow$) or the spin moment ($\uparrow\downarrow$). Nonzero anisotropy is obtained for one and three electrons per doublet. A likely candidate for strong anisotropy is the $|xz\rangle$ and $|yz\rangle$ doublet at an ideal surface layer (Fig. 5), which yields a second-order anisotropy axis perpendicular to the surface. In the relevant limit of strong second-order crystal-field interaction, the doublet lies above the $|z^2\rangle$ level and is, in the Mn^{2+} low-spin state, occupied by three electrons. The situation is reminiscent of the well-known Co^{2+} anisotropy in $(\text{Fe}_{3-x}\text{Co}_x)\text{O}_4$, except for the different position of the doublet and the $3d^6$ high-spin configuration of the Co.¹⁸

This mechanism explains why MnO nanoparticles can have strong atomic-scale surface anisotropy not observed in NiO. In perfectly symmetric nanoparticles, opposing faces would cancel, resulting in no anisotropy. The breaking of symmetry required for this mechanism is provided instead by defects such as steps, interstitial atoms and vacancies.

Using the relationship $KV/k_B T_B = 25$, where K is the anisotropy and V is the nanoparticle volume from TEM, the anisotropies corresponding to the measured peak temperatures are $1.58(\pm 0.07) \text{ kJ/m}^3$ (sample C), $8.08(\pm 0.30) \text{ kJ/m}^3$ (sample B), and $35.27(\pm 0.90) \text{ kJ/m}^3$ (sample A). To evaluate the magnetocrystalline anisotropy, we take into account that intrasublattice and intersublattice exchange interactions in

MnO, as characterized by $T_N=118$ K and $\Theta=-510$ K, are much larger than the Zeeman and anisotropy energies per atom, which are of the order of 1 K or less for fields of a few kOe. The exchange ensures a fairly rigid spin coupling on a scale of a few nanometers and means that the magnetic anisotropy can be averaged safely on a local scale.¹²

The small anisotropy of bulk MnO [on the order of 0.028 kJ/m³ (Ref. 19)] cannot explain the observed blocking behavior. The anisotropy estimated from T_p is three orders of magnitude larger than the bulk value, which is consistent with the relatively large coercivity observed. The anisotropy at any surface site is a complicated nonlinear function of the d -level crystal splitting and hybridization. The resulting anisotropy is random and, without detailed knowledge of the atomic positions, impossible to calculate. The anisotropy is affected further by the capping ligand (an alkyl chain carboxylic acid), which could potentially compensate for some undercoordinated surface Mn²⁺ ions. These factors preclude exact determination of the magnitude and direction of the anisotropy, which generally corresponds to a nonuniaxial ellipsoid with three unequal principal axes and with arbitrary orientation.¹⁰

To estimate the magnitude of the surface anisotropy, we start from perturbation theory, as originally developed by Bloch and Gentile.²¹ The approach considers the spin-orbit coupling λ , about 0.05 eV for the magnetic $3d$ elements, as a small perturbation to the leading crystal-field and hopping contributions ($E_o > 1$ eV). In lowest order (second order), the anisotropy is obtained by evaluating the perturbed energy levels,

$$\delta E_i = -\lambda^2 \sum_j \frac{\langle i | \mathbf{L} \cdot \mathbf{S} | j \rangle^2}{E_j - E_i}, \quad (1)$$

where the E_i are the unperturbed crystal-field (or band-structure levels) and $\Delta E = E_j - E_i \sim E_o$. This equation shows that the magnitude of the second-order anisotropy is proportional to the square of the spin-orbit coupling. Experimentally determined typical anisotropies in $3d$ -based magnets with strong deviations from cubic symmetry are between about 300 kJ/m³ (hexagonal ferrites) and 5000 kJ/m³ (YCo₅).

We parametrize the random surface anisotropy by $\sum_i K_i = 0$ and $\sum_i K_i^2 = N_s K_o^2$, or $\langle K \rangle = 0$ and $\langle K^2 \rangle = K_o^2$. Here N_s is the number of Mn surface atoms and the summation extends from $i=1$ to $i=N_s$. The quantity $\pm K_o$ is the specific anisotropy energy per atomic volume contributing to the energy barrier including, in general, subsurface corrections. The \pm sign means that the anisotropy contribution of the i th atom is easy axis (energy-barrier enhancement) if positive or easy plane (energy-barrier reduction) if negative. When the net anisotropy becomes negative, the magnetization switches into the basal plane of the anisotropy ellipsoid, and the energy is given by the corresponding in-plane anisotropy; however, due to the pronounced nonuniaxial character of the anisotropy, the magnitude of the in-plane anisotropy is comparable to that in any of the two other planes, and the above analysis remains valid. For complete randomness (no

anisotropy correlations due to steps), the net anisotropy of the particle is

$$K_{\text{eff}} = \frac{\sqrt{N_s}}{N} K_o, \quad (2)$$

where N is the total number of Mn atoms. If the anisotropies of the surface atoms were ideally correlated (no surface disorder), then $K_{\text{eff}} = N_s K_o / N$. Considering the smallest particles and taking $K_o = 2000$ kJ/m³ (Ref. 17), we obtain $K_{\text{eff}} = 4.5$ kJ/m³ for complete randomness and $K_{\text{eff}} = 254$ kJ/m³ for no disorder. Our experimental value of 35 kJ/m³ is intermediate, indicating some anisotropy correlations at features such as edges and steps.

The larger particles obey the qualitative trend of Eq. (2). K_{eff} decreases with increasing particle size; however, the effect is difficult to judge as a function of particle size, because K_o also depends on particle size. Physically, the fractions of certain types of surface atoms change, with highly asymmetric or random surface sites more common in small particles. There is some dispersion in the particle size; however, the distributions are narrow enough and the mean sizes span a broad enough range that it is unlikely that the size distribution significantly affects the order-of-magnitude estimates presented here.

IV. DISCUSSION AND CONCLUSIONS

In the preceding section, we have ascribed the behavior of the MnO nanoparticles to the strongly noncubic crystal field at the surface of the particles. This mechanism is different from the bulk MnO high-spin–low-spin transition due to high pressure, where the bands are broadened due to the reduced interatomic distance, but with the cubic anisotropy preserved.²⁰ In the present system, the lattice parameter remains nearly unchanged with particle size, with the primary change being the disruption of symmetry at the nanoparticle surface.

An intriguing feature of the derivation of Eq. (2) is the replacement of the summation over $\lambda^2/\Delta E$ by some average λ^2/E_{eff} , so that the anisotropy energy per $3d$ atom is $K_{\text{at}} = \lambda^2/E_{\text{eff}}$.²² The random character of the energy levels, however, may give rise to very small energy-level differences $\Delta E \sim E_j - E_i$ [as in instance III of Fig. 4(b)], and we then must consider high-order terms. Comparison of $K_{\text{at}} = \lambda^2/\Delta E$ with the exact solution for a simple two-level model^{17,23} suggests the form

$$K_{\text{at}} = \frac{1}{2} (\sqrt{\Delta E^2 + 4\lambda^2} - \Delta E). \quad (3)$$

For large ΔE , this equation reproduces $K_{\text{at}} = \lambda^2/\Delta E$. For small ΔE , K_{at} does not diverge but approaches a maximum value λ , corresponding to the full exploitation of spin-orbit coupling in systems with unquenched orbital moment.²³ Approximating the level splitting by a rectangular distribution with $P(\Delta E) = 1/E_o$, integrating over ΔE , and focusing on the relevant limit $E_o \gg \lambda$ we obtain

$$K_{\text{at}} = \frac{\lambda^2}{E_o} \left[\frac{1}{2} + \ln \left(\frac{E_o}{\lambda} \right) \right]. \quad (4)$$

This rough estimate shows that structural randomness yields only moderate deviations from second-order perturbation theory, in the form of a logarithmic correction. This situation is different from that encountered in itinerant magnets, especially in low-dimensional magnets²⁴ where peaks in the density of states may yield strong corrections ($K_{\text{at}} \sim \lambda$).

In conclusion, the effects of crystal-field splitting and level occupancy due to surface defects produce a significant anisotropy change in MnO nanoparticles. The anisotropy is not only stronger than the bulk MnO anisotropy, but also more pronounced than that of isostructural NiO nanoparticles. The change is explained as a crystal-field effect due to

disorder that allows a high-spin–low-spin transition in MnO not possible in NiO. This explanation is consistent with the observed anomalous increase of the peak temperature in the zero-field-cooled magnetization with decreasing nanoparticle size. Finally, the proposed mechanism and its band-structure generalization may be relevant to other disordered magnetic materials.

ACKNOWLEDGMENTS

The authors acknowledge support from the National Science Foundation (Grant No. DMR-0504706 and CAREER Grant No. DMR-0348938), and MRSEC grants to the University of Nebraska Lincoln (Grant No. DMR-0213808) and Columbia University (Grant No. DMR-0213574).

*Current address: Los Alamos National Laboratory, P. O. Box 1663, MS J567, Los Alamos, NM 87544.

¹G. H. Lee, S. H. Huh, J. W. Jeong, B. J. Choi, S. H. Kim, and H. C. Ri, *J. Am. Chem. Soc.* **124**, 12094 (2002).

²W. S. Seo, H. H. Jo, K. Lee, B. Kim, S. J. Oh, and J. T. Park, *Angew. Chem., Int. Ed.* **43**, 1115 (2004).

³M. Ghosh, K. Biswas, A. Sundaresan, and C. N. R. Rao, *J. Mater. Chem.* **16**, 106 (2006).

⁴R. H. Kodama and A. E. Berkowitz, *Phys. Rev. B* **59**, 6321 (1999).

⁵R. H. Kodama, A. E. Berkowitz, E. J. McNiff, Jr., and S. Foner, *Phys. Rev. Lett.* **77**, 394 (1996).

⁶R. H. Kodama, S. A. Makhlof, and A. E. Berkowitz, *Phys. Rev. Lett.* **79**, 1393 (1997).

⁷S. D. Tiwari and K. P. Rajeev, *Phys. Rev. B* **72**, 104433 (2005).

⁸S. D. Tiwari and K. P. Rajeev, *Thin Solid Films* **505**, 113 (2006).

⁹U. Gradmann, in *Handbook of Magnetic Materials*, edited by K. H. J. Buschow (Elsevier, Amsterdam, 1993), Vol. 7, p. xi.

¹⁰D. Sander, R. Skomski, C. Schmidhals, A. Enders, and J. Kirchner, *Phys. Rev. Lett.* **77**, 2566 (1996).

¹¹J. G. Gay and R. Richter, *Phys. Rev. Lett.* **56**, 2728 (1986).

¹²R. Skomski, *J. Phys.: Condens. Matter* **15**, R841 (2003).

¹³M. Yin and S. O'Brien, *J. Am. Chem. Soc.* **125**, 10180 (2003).

¹⁴E. Stryjewski and N. Giordano, *Adv. Phys.* **26**, 487 (1977).

¹⁵L. F. Mattheiss, *Phys. Rev. B* **5**, 306 (1972).

¹⁶A. H. Bethe, *Ann. Phys.* **3**, 133 (1929).

¹⁷R. Skomski and J. M. D. Coey, *Permanent Magnetism* (Institute of Physics, Bristol, 1999).

¹⁸J. C. Slonczewski, *Phys. Rev.* **110**, 1341 (1958).

¹⁹M. S. Jagadeesh and M. S. Seehra, *Phys. Rev. B* **23**, 1185 (1981).

²⁰R. E. Cohen, I. I. Mazin, and D. G. Isaak, *Science* **275**, 654 (1997).

²¹F. Bloch and G. Gentile, *Z. Phys.* **70**, 395 (1931).

²²Note that $K_{\text{at}} = K_o V_o$, where $V_o = 21.8 \text{ \AA}^3$ is the crystal volume per Mn atom.

²³R. Skomski, *Simple Models of Magnetism* (University Press, Oxford, 2007).

²⁴G. H. O. Daalderop, P. J. Kelly, and M. F. H. Schuurmans, *Phys. Rev. B* **50**, 9989 (1994).